Journal of Photochemistry and Photobiology A: Chemistry 198 (2008) 169–178

Contents lists available at ScienceDirect

Journal of Photochemistry and Photobiology A: Chemistry

journal homepage: www.elsevier.com/locate/jphotochem

Radiation field modeling of multi-lamp, homogeneous photoreactors

Gustavo E. Imoberdorf[1], Fariborz Taghipour, Madjid Mohseni*

Department of Chemical and Biological Engineering, University of British Columbia, 2360 East Mall, Vancouver, BC, Canada VT6 1Z3

ARTICLE INFO

Article history:
Received 11 September 2007
Received in revised form 5 March 2008
Accepted 11 March 2008
Available online 18 March 2008

Keywords:
Modeling
Radiation
Multi-UV lamps
UV-reactor
Monte Carlo method

ABSTRACT

For modeling and optimization of photoreactors, knowing radiation distribution inside the reactor is essential because the kinetics of photochemical and photocatalytic reactions are strongly dependent on the local incident radiation. In this work, a Monte Carlo multi-lamp radiation model is proposed. The model takes into account the reflection on the surface of the lamps, the refraction in the quartz lamp envelope, as well as the adsorption and the isotropic re-emission of radiation in the mercury vapor of the lamp. To quantify the shadowing effect among the lamps, the effective transmittance through a UV-lamp turned on, a lamp turned off, and a lamp quartz envelope have been measured. For validation purposes, experimental measurements have been performed using one, two, and three lamps. The model predictions show good agreement with the experimental results. Finally, in order to simplify the numerical solution of the model, the validity of assuming the lamps 100% opaque and 100% transparent have been analyzed.

1. Introduction

Safe drinking water is essential to human health, as well as for economic and industrial development. Chlorination is the most common technique for dinking water disinfection because chlorine is a highly oxidizing chemical that inactivates most of pathogenic microorganisms. However, formation of undesirable chlorination by-products, such as mutagenic and carcinogenic agents [1,2], has prompted the application of alternative disinfection methods that could minimize environmental and public health impacts. The use of ultraviolet (UV) irradiation is an effective alternative for water disinfection [3–7]. For industrial or large-scale applications, multi-lamp UV reactors are particularly useful because they allow disinfection of greater flow rates of water than those obtained in single-lamp reactors.

There are a number of studies aimed at the development of integrated models for predicting the performance of UV-photoreactors [8–11]. Knowing the radiation field is essential for developing accurate models because microorganism inactivation rates are strongly dependent on the local incident radiation [12,13]. Besides, since the existence of dark zones in UV-photoreactors may significantly reduce their performance [14], radiation models could be used to optimize UV-photoreactor designs by improving the radiation distribution in the reactors. Errors in predicting the radiation flux in photoreactors will affect directly the accuracy of the prediction of the reactor efficiency, whether the reactor is applied to disinfection or to pollutants degradation.

The fundamental equation describing the propagation of photons in a given domain is the radiative transfer equation. Unfortunately, this equation can be solved analytically only in a few simplified cases [15] and most real applications require numerical methods [16]. The most widespread numerical methods used to solve the radiative transfer equation are the Discrete Ordinate (DO) method and the Monte Carlo (MC) method. Besides, Computational Fluid Dynamics (CFD) allows for modeling simultaneously the hydrodynamics of the system, the kinetics of chemical reactions, and the radiative energy transfer [17]. The MC method has been successfully applied to solve the radiation field in different geometries, such as monolith photocatalytic reactors [18,19], fixed bed photocatalytic reactors [20,21], and photocatalytic slurry reactors [22–24].

Solving the radiative transfer equation inside a photoreactor requires the knowledge of the boundary conditions, which can be evaluated by using lamp emission models [25]. The most commonly employed lamp emission models include the Multiple Point Source Summation (MPSS) model, where the lamp emission is modeled as a finite number of equally spaced point sources along the axis of the lamp [26]; an expanded emission model based on MPSS, which takes into account the refraction and reflection effects occurring at the quartz sleeves that generally are used in UV-photoreactors [27]; the Line Source with Spherical Emission (LSSE) model, which considers the lamp as a 1D line emitting radiation isotropically in all directions [26,28]; the Line Source with Diffused Emission

* Corresponding author. Tel.: +1 604 822 0047; fax: +1 604 822 6003.
E-mail address: mmohseni@chml.ubc.ca (M. Mohseni).
[1] Permanent address: INTEC, Instituto de Desarrollo Tecnológico para la Industria Química (Universidad Nacional del Litoral and CONICET), Güemes 3450, (S3000GLM) Santa Fe, Argentina.

1010-6030/$ – see front matter © 2008 Elsevier B.V. All rights reserved.
doi:10.1016/j.jphotochem.2008.03.006

Nomenclature

A	area (cm^2)
$e_{envelope}$	wall thickness of the quartz envelope (cm)
E	radiative energy associated to a given photon (mW)
G	local incident radiation ($mW\,cm^{-2}$)
I	specific radiation intensity ($mW\,cm^{-2}\,sr^{-1}$)
K_{Hg}	spectral absorption of the mercury vapor (cm^{-1})
L_{lamp}	lamp length (cm)
n	reflection index relative to air, dimensionless; also the number of photons or lamps
$\underline{n}_s$	unit vector normal to a given surface
P_{lamp}	spectral emission power of the lamp (W)
q	local net radiation flux ($W\,cm^{-2}$)
r	radial coordinate (cm)
r_{lamp}	lamp external radius (cm)
R_1–R_7	uniformly distributed random numbers
T	transmittance (%)
x	rectangular coordinate (cm)
$\underline{x}$	position vector (cm)
y	rectangular coordinate (cm)
z	rectangular coordinate (cm)

Greek letters

Ω	solid angle (sr)
$\underline{\Omega}$	unit vector in the direction of propagation of a beam
ζ	distance traveled by a given photon (cm)
θ	polar angle (rad)
λ	wavelength (nm)
Φ	quantum efficiency of the absorption/re-emission process
ρ	local reflectivity
ϕ	azimuthal angle (rad)
φ	angle between two given vectors (rad)

Subscripts

det	relative to the UV detector
Hg	relative to the mercury vapor inside the UV-lamps
in	relative to the incident beam
n	relative to the normal vector to a given surface
$p-d, \underline{x}$	relative to the photons that reach the detector surface located at a given position
s	relative to a given surface
tr	relative to the transmitted beam
λ	wavelength

Superscripts

*	relative to the previous value in an iterative process

(LSDE) model, which is similar to the LSSE model, but assumes the lamp as a line emitting radiation diffusely following cosine law [29,30]; and the Extensive Source with Volumetric Emission (ESVE) model, which considers that the radiation is emitted uniformly in the three-dimensional volume of the lamp [31]. Quan et al. [32] compared the values of incident radiation predicted by LSSE, LSDE, and ESVE models against experimental results. They concluded that these models predict accurately the radial distribution of light, but the accuracy of LSDE and ESVE models is slightly higher than that of the LSSE model.

For modeling multi-lamp systems, it is necessary to consider not only the lamp emission model, but also the behavior of the radiation emitted by one lamp that reaches the other ones. Under such conditions, reflection and refraction effects are important. When radiation reaches an interface between two media of different refractive indices (i.e., the lamp envelope), a fraction of the radiant energy is reflected and the rest passes through the interface toward the second medium. The ratio of the reflected and refracted radiation depends on the incident angle of the radiation and on the ratio of refractive indices of the two media. Besides, the trajectory of radiation beams transmitted through the lamp envelope will be modified because of the refraction effects in the curved surfaces of the lamp envelopes. The importance of reflection and refraction effects in quartz sleeves has been reported by Bolton [27]. These effects are particularly important when propagation media has a high transmittance, which is generally the case in water disinfection systems [27]. With respect to the possible absorption of UV radiation in the quartz envelope, this effect can be neglected because the volumetric absorption coefficient of quartz at 253.7 nm is practically zero.

Since the MPSS, the LSSE, and LSDE models do not consider the lamps as three-dimensional objects, which are required to model shadows or reflections, they could not be employed to predict multi-lamp interactions. Regarding the ESVE model, neither reflection/refraction effects on/in the lamp envelope nor absorption/re-emission effects in the mercury vapor inside the lamp are considered. Moreover, according to the assumption of the ESVE model [31], the lamps would be completely transparent to UV radiation.

There are only few articles in the open literature focused on multi-lamp UV-photoreactor modeling. Yokota and Suzuki [30] studied the radiation field in a multi-lamp photoreactor. They used the LSDE model, with the assumption that the lamps are completely opaque, and studied the radiation distribution. They focused on the analysis of the optimal location of two, three, and four lamps in multi-lamp systems in order to achieve maximum averaged incident radiation. Jin et al. [14] analyzed the reflection and shadowing effects that take place in multi-lamp systems by using experimental results. The experimental set-up was comprised of four low-pressure UV lamps forming a square pattern. Actinometric techniques were employed for measuring the local incident radiation at different positions. Experimental results were compared with the numerical values predicted by the two radiation models, in which the lamps were considered completely opaque to UV radiation, and the reflection on the lamp surfaces was neglected. Modeling predictions were, in general terms, significantly higher than their experimental results, and this was attributed to the saturation of the actinometer solution. The authors [14] concluded that shadowing effects can significantly affect radiation distribution in a UV reactor, reducing the global performance of the reactor on the microorganism inactivation. Pareek [33] studied the radiation distribution in a two-lamp photoreactor by using a CFD software (Fluent), focusing only on the analysis of the slurry photocatalytic reactors.

In this work, a multi-lamp radiation model based on the MC approach is developed. This model takes into account the radiation, reflection and refraction effects on/in the lamp envelope, and the interaction of radiation with mercury vapor. The model predictions were compared to experimental results obtained using a radiometer located at different positions in a multi-lamp setup. Different experiments were conducted using one, two, and three lamps, as well as a lamp envelope. Finally, the validly of some additional assumptions have been analyzed in order to simplify the numerical solution of the model.

2. Experimental set-up and procedure

The experimental measurements were carried out in a cubical chamber (Fig. 1a), capable of housing several UV lamps and/or

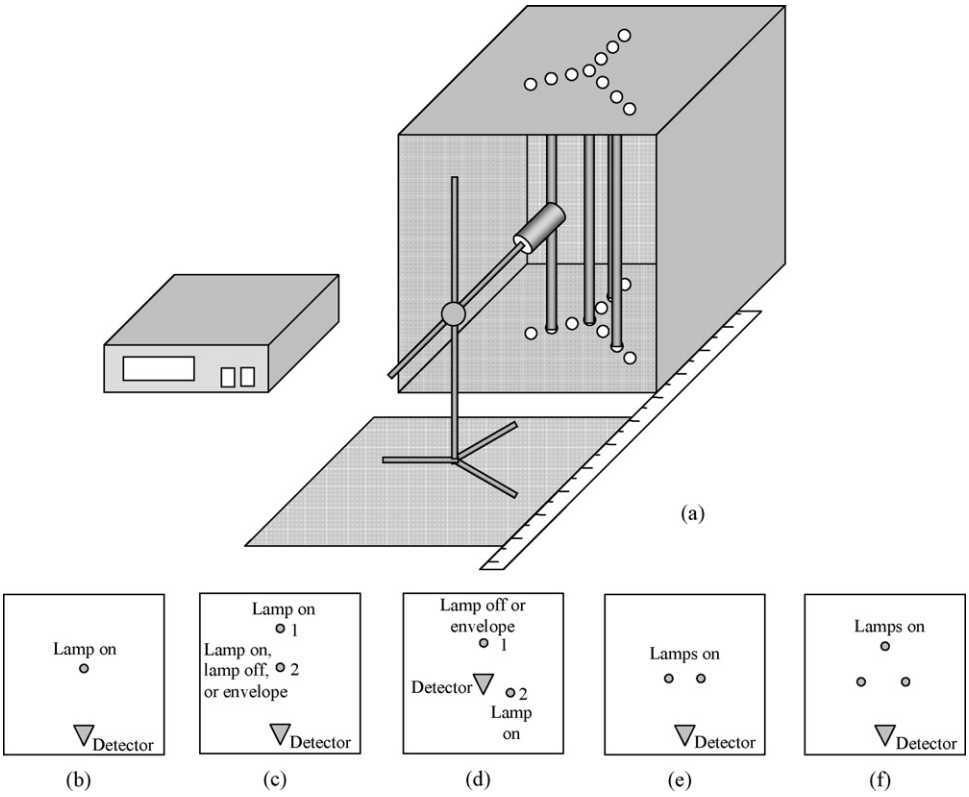

Fig. 1. Experimental set-up: multi-lamp chamber.

lamp quartz envelopes at different locations. The internal walls of the chamber were covered with opaque black paint in order to minimize the reflection of radiation, reducing the undesirable interference of such effect on the radiation flux measurements. Low-pressure mercury lamps (GPH357T5L/4P, Light Sources Inc.) were used as a source of UV radiation ($\lambda = 253.7$ nm). A lamp quartz envelope was also employed in some of the experiments to investigate the effect of the reflection/refraction on/in the quartz envelope and to distinguish between these effects and those associated with the mercury vapor inside the UV-lamps. The lamp envelope employed was obtained from a UV-lamp, after the mercury vapor was removed, and the envelope surface was carefully cleaned. The local radiative flux was measured at different positions using a research radiometer (IL 1700, SED240 sensor, NS254 filter, International light). The detector of the radiometer was fixed on a mobile platform, which was aligned in relation to the center point of the measurement chamber (Fig. 1a). When the lamps were turned on, the open face of the measurement chamber was covered with a black fabric to minimize the radiation leaving the measurement zone, and to prevent the external ambient radiation from interfering in the measurements.

The procedure for each experiment was as follows: the radiometer and the lamps were placed in a defined configuration, the open face of the measurement chamber was covered with the black fabric, the lamps were turned on, and after reaching a constant radiometer reading, the value of the radiation flux was recorded. Five sets of experimenters were performed:

(i) One-lamp measurements: the radiation flux emitted by one lamp located at the center of the chamber was measured using the radiometer placed at different distances from the lamp (Fig. 1b).

(ii) Two interposed lamp measurements: to study the shadowing effect, two lamps were arranged in line with the detector at positions 1 and 2 (Fig. 1c), placed at a distance of 5 cm from each other and then both were turned on. Measurements were performed by placing the detector of the radiometer at different positions in line with the lamps. Two analogous sets of measurements were carried out after turning off the lamp placed at position 2 (Fig. 1c), and after replacing this lamp with a lamp quartz envelope.

(iii) Indirect radiation measurements: to study and quantify the effect of mercury vapor inside the UV-lamp on the radiation field, the radiation flux reflected from a UV-lamp or a lamp envelope at different positions opposite to the detector was measured (Fig. 1d). For this set of experiments, the radiometer detector was placed at the center of the chamber; the lamp acting as a radiation source was placed away from the measurement region of the detector (at position 2, Fig. 1d), and was turned on. Measurements of the radiation flux were performed after placing another lamp turned off or a quartz envelope opposite the detector (at position 1, Fig. 1d).

(iv) Two adjacent lamp measurements: to validate the model for a multi-lamp reactor, the UV radiation emitted from two adjacent lamps located opposite the detector was measured with the detector oriented towards the center of the chamber. The configuration of the lamps is shown in Fig. 1e. Additional measurements were carried out, but with the detector oriented to the center of one of the lamps, keeping the other lamp off. This procedure was repeated for the other lamp.

(v) Three lamp measurements: this set of measurements was analogous to that in (iv), but the radiation was emitted from all three lamps, forming a triangular arrangement and placed opposite the detector (Fig. 1f).

Table 1
Experimental measurement of the shadowing effect for the quartz envelope, the lamp turned off and the lamp turned on (Fig. 1c)

Distance (cm)	$q_1(\underline{x})$ lamp 1 on ($mW\,cm^{-2}$)	$q_2(\underline{x})$ lamp 2 on ($mW\,cm^{-2}$)	$q_3(\underline{x})$ lamp 1 on + lamp 2 off ($mW\,cm^{-2}$)	$q_4(\underline{x})$ lamp 1 on + envelope ($mW\,cm^{-2}$)	$q_5(\underline{x})$ lamp 1 on + lamp 2 on ($mW\,cm^{-2}$)	Envelope transmittance (%)	Lamp off transmittance (%)	Lamp on transmittance (%)
2	3.00	7.00	0.871	1.23	7.43	40.83	29.02	14.17
4	2.33	4.17	0.669	0.924	4.39	39.73	28.76	9.60
6	1.88	3.06	0.496	0.738	3.28	39.37	26.47	11.90
8	1.58	2.43	0.385	0.597	2.61	37.75	24.35	11.42
10	1.33	2.14	0.334	0.504	2.33	38.07	25.19	14.43

3. Preliminary discussion: relevant physical effects

The significance of the reflection/refraction/absorption effects on/in the quartz envelope is well established. However, the effect of the mercury vapor inside the lamps is not evident. Prior to presenting the radiation model, the interaction of radiation with mercury vapor is briefly discussed.

When mercury vapor is irradiated with 253.7 nm radiation, mercury atoms can absorb the photons and be promoted to an exited state [34]:

$$Hg\,6(^1S_0) + h\nu_{253.7\,nm} \rightarrow Hg\,6(^3P_1)$$

The $Hg\,6(^3P_1)$ atoms may disappear by re-emitting the radiation at the same wavelength as the one absorbed in the excitation:

$$Hg\,6(^3P_1) \rightarrow Hg\,6(^1S_0) + h\nu_{253.7\,nm}$$

In addition, re-emitted radiation may be re-absorbed (and re-emitted again) by several mercury atoms, until finally the photons leave the system, or are converted into kinetic energy by collisions. The time required for the exited mercury atom to re-emit a photon and restore to the non-exited state is very short, with the lifetime for an isolated atom of $Hg\,6(^3P_1)$ being equal to 1.1×10^{-7} s [34]. The re-emitted radiation will be completely diffused; consequently, this process can be considered, from a mathematical point of view, an elastic isotropic scattering.

The quantum yield of the radiation re-emission process is defined as the ratio of the re-emitted to the absorbed radiation:

$$\Phi = \frac{I_{\text{re-emitted}}}{I_{\text{absorbed}}} \quad (1)$$

In the absence of atomic collisions and other effects, exited mercury $Hg\,6(^3P_1)$ can undergo only this inverse absorption process, resulting the quantum yield of the radiation re-emission equal to unity. This is particularly true for systems containing only mercury vapor at low pressures [35], which is the case for typical low-pressure UV lamps.

In order to define a suitable hypothesis for modeling the interaction between radiation and the mercury vapor, some exploratory experiments were conducted. Two of such experiments were particularly enlightening: (i) the comparative analysis of the effective transmittances obtained with a lamp turned off against those obtained using the lamp quartz envelope (i.e., two interposed lamp measurements, Fig. 1c), and (ii) the comparative analysis of the effective reflectance obtained with a lamp turned off and with the quartz envelope (i.e., indirect radiation measurements, Fig. 1d).

For the two interposed lamp measurements, Table 1 shows the radiative flux obtained from two interposed lamps measurements (Fig. 1c), where there was a lamp on at position 1 and there was a lamp on or off, or a lamp quartz envelope at position 2. The effective transmittances of the lamp turned off and of the quartz envelope were evaluated as the rate of the radiation flux measured before and after placing the lamp and the envelope at position 2 (Fig. 1c), respectively:

$$T_{\text{lamp off}}(\%) = \frac{q_3(\underline{x})}{q_1(\underline{x})} \times 100 \quad (2)$$

$$T_{\text{envelope}}(\%) = \frac{q_4(\underline{x})}{q_1(\underline{x})} \times 100 \quad (3)$$

The effective transmittance of the lamp turned on located at position 2 was calculated by subtracting its own emission ($q_2(\underline{x})$) from the values obtained from the experiment involving both lamps turned on ($q_5(\underline{x})$), and dividing by the emission of the lamp located at position 1 ($q_1(\underline{x})$):

$$T_{\text{lamp on}}(\%) = \frac{q_5(\underline{x}) - q_2(\underline{x})}{q_1(\underline{x})} \times 100 \quad (4)$$

At all the distances, the effective transmittances of the quartz envelope was $39.2 \pm 3.1\%$, which was higher than those of the lamps off and on, where the average effective transmittances were $26.8 \pm 1.6\%$, and $12.3 \pm 0.6\%$, respectively. The results indicate that the effect of the mercury vapor is only present for the lamp and not for the quartz envelope. Besides, as expected, the transmittances obtained with the lamp turned on were lower than those obtained with the lamp turned off. The decrease of the effective transmittance of the lamp when it is turned on can be attributed to the increase of the vapor pressure of mercury, which is the consequence of the electrical arc and the temperature increase.

A complementary study was performed with the objective of analyzing the reflection effects of the lamp envelope and the possible contribution of radiation re-emitted by the mercury vapor of the lamps. For this study, a lamp was placed at position 2 (Fig. 1d), beside the radiometer whereby the detector was not receiving the direct radiation emitted from this lamp. At different distances from the detector, another lamp or a lamp envelope was placed (position 1), then the lamp at position 2 was turned on and measurements were taken (the lamp at position 1 was maintained off). The experimental results are summarized in Table 2. When a lamp that is turned off is located opposite the detector (position 1), the radiative flux measured is 250% higher compared to that obtained when the quartz envelope is placed in the same location. This result is in agreement with the assumption that mercury can absorb and re-emit UV radiation, showing that this effect is significant, even when the lamp is off. In this way, when a lamp that is turned off is used, the detector is receiving not only the energy associated with the reflection, but also the energy that is re-emitted isotropically by the mercury vapor.

Table 2
Experimental measurements of the reflectance in a quartz envelope and in a lamp turned off

Distance (cm)	L1 on + L2 off ($mW\,cm^{-2}$)	L1 on + envelope ($mW\,cm^{-2}$)
2.5	1.07×10^{-1}	4.20×10^{-2}
5	4.21×10^{-2}	1.75×10^{-2}
7.5	2.04×10^{-2}	8.12×10^{-3}
10	1.11×10^{-2}	4.18×10^{-3}

The above experimental results suggest that the mercury vapor, even at a very low concentration, has an important role in the optical behavior of the lamp. The optical properties of mercury vapor will depend on the wavelength and on the vapor pressure, which also depends on the temperature. In this work, we have estimated the extinction coefficient of mercury vapor at 253.7 nm form experimental results under two conditions: lamp turned on and lamp turned off (no reported values in the open literature are available). As the adsorption-and-re-emission process is isotropic, the final radiation distribution will be practically the same as that obtained using the lamp emission models that consider isotropic emission.

4. Radiation model

4.1. Model description

The radiation model was based on the Monte Carlo (MC) method, taking into account most of the assumptions of the ESVE model [25,31]. In addition, the reflection/refraction effects on/in the quartz envelope and the absorption/re-emission of the mercury vapor were included (Fig. 2). The model assumptions are summarized as follows:

(i) Photons are emitted from locations uniformly distributed over the lamp volume. The probability for a photon to be emitted is the same at any location in the UV-lamp volume, independent of their relative position (without end effects).
(ii) The local radiation energy emitted in the lamp volume is isotropic. Thus, each photon does not have a preferential direction and any direction is equally plausible.
(iii) Photons may be absorbed and re-emitted by the mercury vapor, and the efficiency of this process is considered unity since the pressure of the mercury vapor in the lamp is extremely low.
(iv) All the processes taking place in the lamp, such as emission, absorption, and re-emission are at steady state.
(v) Reflection on quartz envelope is specular and the numerical values of the local angle-dependant reflectivity are evaluated using the Fresnel equation [36].
(vi) Refraction effects, which are also considered as specular, are evaluated using the Snell law [36].
(vii) For the Fresnel equation and the Snell law, the index of refraction values for air, low-pressure mercury vapor, and quartz are 1.00, 1.00 and 1.61, respectively.
(viii) The absorption of the UV radiation in the quartz is negligible at 253.7 nm.

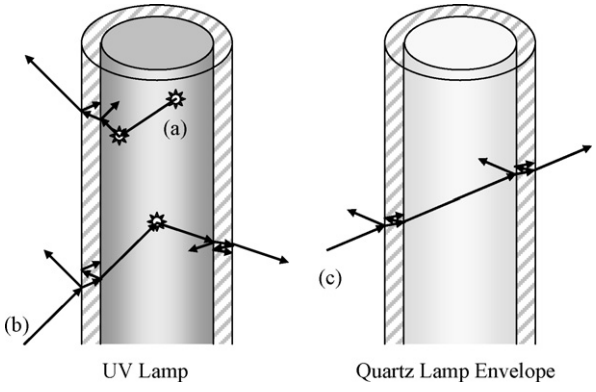

Fig. 2. Schematic representation of photon behavior in UV-lamp and quartz envelope: (a) emission of a photon in the lamp, (b) interaction of a photon with the UV-lamp and (c) interaction of a photon with the lamp envelope. In all the cases, reflection (or multi-reflection) and refraction was taken into account.

(ix) Outside the lamps and within the quartz envelope (i.e., air), photons advance in rectilinear direction until they intercept another surface. Inside the lamps they also advance in rectilinear direction but they can be absorbed and re-emitted by mercury atoms, where they change their propagation direction, in agreement with the random walk model. At the absorption/re-emission point, a new isotropic direction for the propagation of the photon is defined.
(x) All the UV-lamps have the same power emission.

Prior to describing the radiation model, it is necessary to define the local net spectral radiation flux, $q_\lambda(\underline{x})$:

$$q_\lambda(\underline{x}) = \int_\Omega I_\lambda(\underline{x}, \underline{\Omega})\underline{\Omega}\cdot\underline{n}_s \mathrm{d}\Omega = \int_{\theta=0}^{\pi/2}\int_{\phi=0}^{2\pi} I_\lambda(x,y,z,\theta,\phi)\,\mathrm{Sin}\,\theta\,\mathrm{Cos}\,\varphi_n \mathrm{d}\phi\,\mathrm{d}\theta \quad (5)$$

where $I_\lambda(\underline{x}, \underline{\Omega})$ is the spectral specific radiation intensity associated with the energy reaching a given surface at position $\underline{x}$ with direction $\underline{\Omega} = (\theta, \phi, 1)$, $\underline{n}_s$ is the unit vector normal to the surface considered, θ and ϕ are the polar and azimuthal angles, respectively, φ_n is the angle between $\underline{\Omega}$ and $\underline{n}_s$, and $\mathrm{d}\Omega = \sin\theta\,\mathrm{d}\phi\mathrm{d}\theta$ is a differential solid angle around the direction $\underline{\Omega}$. The incident radiation is defined as follows:

$$G_\lambda(\underline{x}) = \int_\Omega I_\lambda(\underline{x}, \underline{\Omega})\mathrm{d}\Omega = \int_{\theta=0}^{\pi/2}\int_{\phi=0}^{2\pi} I_\lambda(x,y,z,\phi,\theta)\,\mathrm{Sin}\,\theta\,\mathrm{d}\phi\,\mathrm{d}\theta \quad (6)$$

In general terms, the MC method applied to obtain the local net spectral radiation flux consists of tracking the trajectory of a great number of photons, in order to compute the percentage of photons that reach a given surface. The photon tracking is based on the laws of geometric optics (such as the Snell refraction law and the Fresnel reflectivity equation). The energy carried by each photon (E_{photon}) is calculated as the rate of the total energy emitted by the lamps to the number of photons considered:

$$E_{photon} = \frac{P_{lamp,\lambda} n_{lamps}}{n_{photons}} \quad (7)$$

where $P_{lamp,\lambda}$ is the spectral emission power of the lamp, n_{lamps} is the total number of lamps in the system, and $n_{photons}$ is the total number of photons considered. At this point, it is important to mention that the term "photon" not only has the literal meaning, but also means the basic unit of radiative energy employed in the MC method, according to Eq. (7). After tracking the trajectory of all the photons considered, the local net spectral radiation flux can be calculated by means of

$$q_\lambda(\underline{x}) = E_{photon}\frac{n_{p-d,\underline{x}}}{A_{det}} = \frac{P_{lamp} n_{lamps}}{A_{det}}\frac{n_{p-d,\underline{x}}}{n_{photons}} \quad (8)$$

where A_{det} is the sensitive surface area of the detector and $n_{p-d,\underline{x}}$ is the number of photons that reach this surface at different positions, which is calculated after the photon tracking.

The MC algorithm developed is summarized in Fig. 3. According to the MC model, a plausible emission point as well as a plausible propagation direction must be defined for each photon. Considering that the lamps have the same effective emission power, the particular lamp where a photon is emitted can be defined stochastically by using one random number:

$$n_{lamp,i} = \mathrm{Int}(R_1 n_{lamp}) + 1 \quad (9)$$

where Int(_) is the integer function, which calculates the integer part of the argument, and R_1 is a uniformly distributed random number. When only one lamp is considered, the numerical value

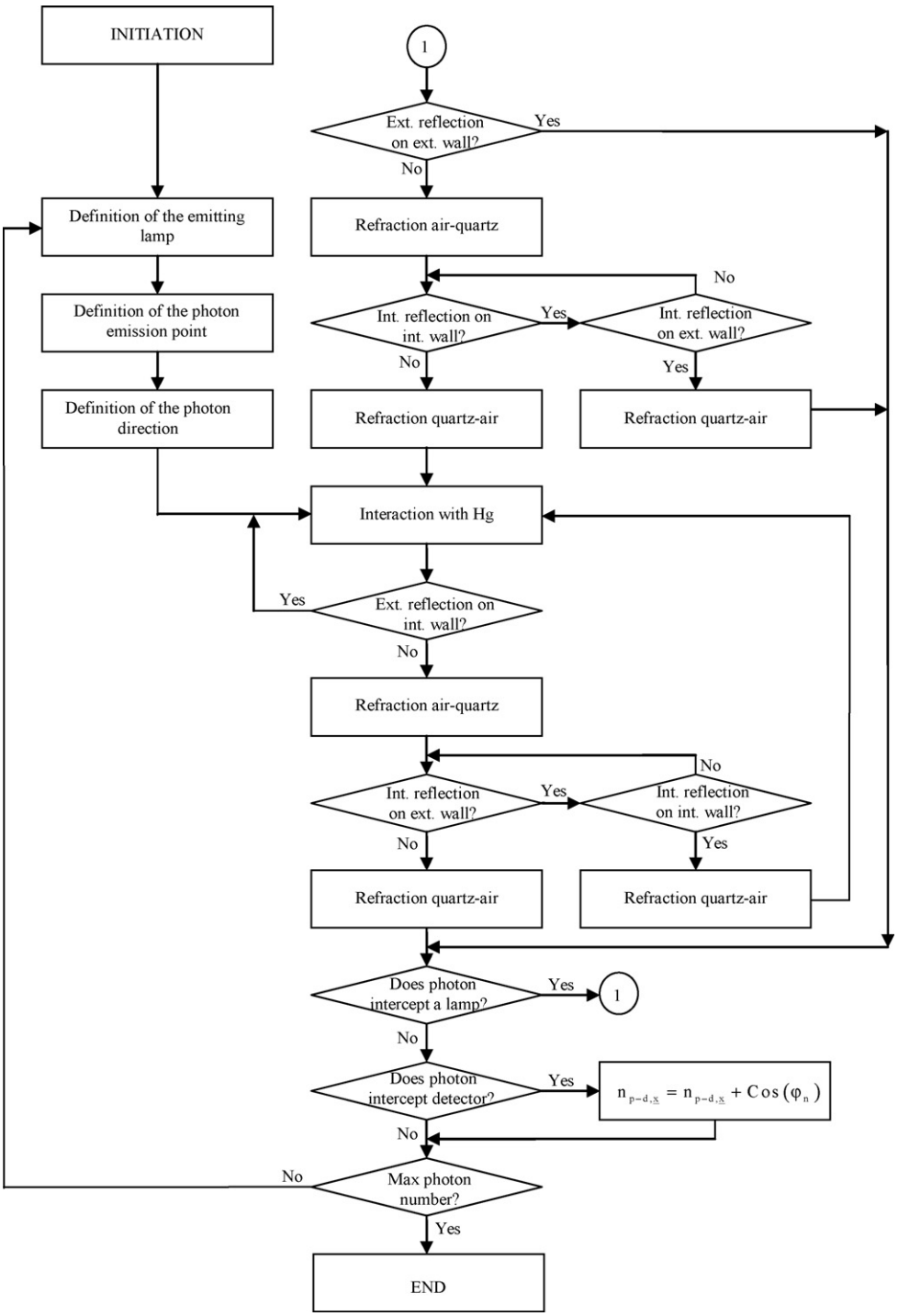

Fig. 3. Simplified representation of the Monte Carlo algorithm employed to evaluate the radiation flux at different positions.

of Eq. (9) is equal to unity. Since the probability for a photon to be emitted is assumed uniform in the lamp volume, the emission point can be defined stochastically by using three random numbers as follows:

$$x_{\text{photon},i} = x_{\text{lamp}}(n_{\text{lamp},i}) + (r_{\text{lamp}} - e_{\text{envelope}})\sqrt{R_2}\,\text{Cos}(2\pi R_3) \quad (10)$$

$$y_{\text{photon},i} = y_{\text{lamp}}(n_{\text{lamp},i}) + (r_{\text{lamp}} - e_{\text{envelope}})\sqrt{R_2}\,\text{Sin}(2\pi R_3) \quad (11)$$

$$z_{\text{photon},i} = L_{\text{lamp}}\left(R_4 - \frac{1}{2}\right) \quad (12)$$

where $x_{\text{lamp}}(n_{\text{lamp,i}})$ and $y_{\text{lamp}}(n_{\text{lamp,i}})$ are the coordinates of the lamp center that emits the ith photon, r_{lamp} is the lamp radius, e_{envelope} is the wall thickness of the quartz envelope, and L_{lamp} is the lamp length. In a similar way, the propagation direction of the current photon can be stochastically defined by using two random numbers:

$$\phi_{\text{photon},i} = 2\pi R_5 \quad (13)$$

$$\theta_{\text{photon},i} = \text{Sin}^{-1}(2R_6 - 1) + \frac{\pi}{2} \quad (14)$$

The emitted photons are inside a participative medium (mercury vapor); therefore, they could be absorbed and re-emitted. The distance that photons travel in a participative medium until they are absorbed (ζ) can be defined stochastically using the following equation:

$$\zeta = -\frac{\mathrm{Log}(1 - R_7)}{K_{\mathrm{Hg}}} \tag{15}$$

where K_{Hg} is the absorptivity of the mercury vapor at 253.7 nm. This optical property for the two cases of lamp turned on and off was estimated in this work, from two sets of experiments, and was further validated with experimental values obtained under different conditions.

Using Eq. (15) and geometric optics, it is possible to track the photon trajectory until the point where it is absorbed. Nevertheless, Eq. (15) is only valid for photons traveling in a pseudo-homogeneous medium, without changes of the propagation medium. Since the lamp is a finite system, photons may reach the lamp internal surface without being absorbed. For this reason, it is necessary to check if the photon trajectory takes place completely in the mercury vapor inside the lamp. In such situation, the current photon is considered to travel the distance calculated using Eq. (15). Then, at this new location in the mercury vapor, it is absorbed and re-emitted, where the new propagation direction can be calculated by applying Eqs. (13) and (14). Otherwise, when the photon reaches the lamp surface, it may be either reflected or refracted. Using geometric optics, it is possible to track the trajectory of the photon and calculate the position and direction vectors at the interception point. Knowing these vectors allows for calculating the angle between the direction of the photon and the normal vector to the internal face of the lamp, which is used to calculate the local reflectivity by means of the Fresnel equation [36]:

$$\rho(\varphi_{\mathrm{in}}, \varphi_{\mathrm{tr}}) = \frac{1}{2}\left[\frac{n_1 \mathrm{Cos}(\varphi_{\mathrm{in}}) - n_2 \mathrm{Cos}(\varphi_{\mathrm{tr}})}{n_1 \mathrm{Cos}(\varphi_{\mathrm{in}}) + n_2 \mathrm{Cos}(\varphi_{\mathrm{tr}})}\right]^2 + \frac{1}{2}\left[\frac{n_1 \mathrm{Cos}(\varphi_{\mathrm{tr}}) - n_2 \mathrm{Cos}(\varphi_{\mathrm{in}})}{n_1 \mathrm{Cos}(\varphi_{\mathrm{tr}}) + n_2 \mathrm{Cos}(\varphi_{\mathrm{in}})}\right]^2 \tag{16}$$

where φ_{in} and φ_{tr} are the angles between the normal vector of the detector surface to the incident and transmitted (refracted) vectors, respectively, and n_1 and n_2 are the reflection indices of the media. The result of the interaction of the photon with any surface is defined stochastically by a random number:

$$R_8 \begin{cases} \leq \rho(\varphi_{\mathrm{in}}, \varphi_{\mathrm{tr}}) \Rightarrow \text{reflection} \\ > \rho(\varphi_{\mathrm{in}}, \varphi_{\mathrm{tr}}) \Rightarrow \text{refraction} \end{cases} \tag{17}$$

When the photon is reflected, the new propagation direction is evaluated considering specular reflection and the plausible distance for absorption is calculated using Eq. (15). This process is repeated until the photon leaves the mercury vapor through the lamp envelope (see Fig. 3). When the photon is refracted, the change of the direction in quartz phase is evaluated using the Snell law. Photons traveling through the quartz will not change their direction nor be absorbed until they reach the internal or external surface of the envelope, where the calculus methodology previously described is applied. This complex series of emission/absorption/re-emission/refection/refraction events will take place until the photon finally leaves the UV-lamp.

Once outside the lamp, photons will travel rectilinearly until they are intercepted by another UV-lamp, the radiometer detector, or the test chamber walls. In this case, where the external medium is non-participative, photons are not absorbed by the medium. When a photon reaches the external surface of a lamp, it can be reflected or refracted. Again, the complex series of emission/absorption/re-emission/refection/refraction events are considered (see Fig. 3). This situation is solved in a similar way as described previously.

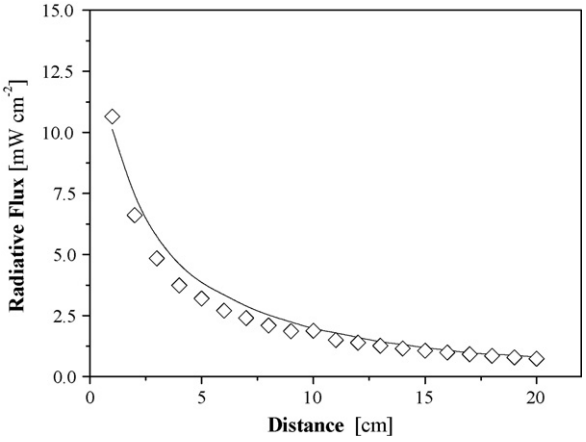

Fig. 4. Radiation flux obtained with one lamp: (◊) experimental values, and (–) predicted Monte Carlo values.

The purpose of the ray tracking process previously described is to quantify the amount of photons that would reach the detector placed at a given position. Knowing the origin point and direction of photons outside the lamps allows for calculating whether the photons reach the detector or not. In order to properly interpret the experimental results, the sensitive part of the detector was modeled as a 1.0 cm diameter circle, 1.5 cm beneath the detector face [37]. The number of photons that reach the detector surface when located at a given position ($\underline{x}$) is stored in the following way:

$$n_{\mathrm{p-d},\underline{x}} = n^*_{\mathrm{p-d},\underline{x}} + \mathrm{Cos}(\varphi_{\mathrm{n}}) \tag{18}$$

where the asterisk refers to the previous value and φ_{n} is the angle between the trajectory of the photon and the normal vector of the detector surface. Note that the contribution of every photon to the total amount of energy that reaches the detector is considered lower than unity because, according to information provided by the manufacturer, the sensitivity of the detector decreases with the cosine of φ_{n}. The possibility for each photon to reach different detection locations is explored.

Finally, once the trajectories of all the photons are tracked, the radiation flux corresponding to each detector position is calculated using Eq. (8).

The mathematical model was solved with an ad hoc developed FORTRAN program, based on the solution algorithm schematically shown in Fig. 3. The calculations were done with a 1.60-GHz Pentium III Processor, and the time required for a typical run, considering 10^5 photons, is on the order of 10 min.

4.2. Model evaluation

4.2.1. One lamp

Fig. 4 shows the experimental and predicted values of the radiation flux emitted by one lamp versus the distance from the center of the lamp (Fig. 1b). As expected, the maximum value of the radiation flux is located close to the lamp, where a steep gradient of the radiation flux can be noted. As the distance of the detector from the lamp increases, lower values of radiation flux are obtained as a consequence of the divergence of the radiation beams. The model predictions show good agreement with the experimental measurements in the range analyzed.

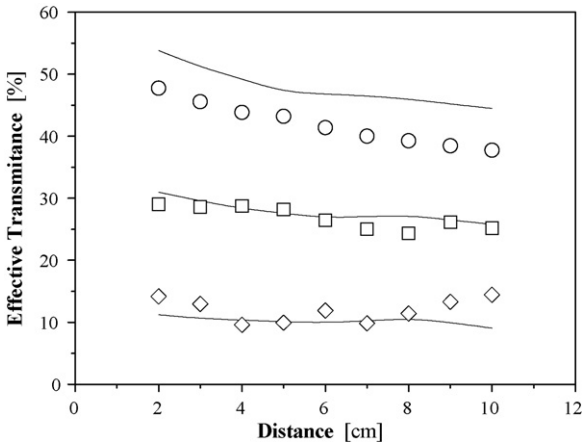

Fig. 5. Effective transmittance obtained with two lamps (shadowing effect). Experimental results obtained by using (○) a lamp envelope, (□) a lamp turned off, (◊) a lamp turned on, and (–) predicted Monte Carlo values.

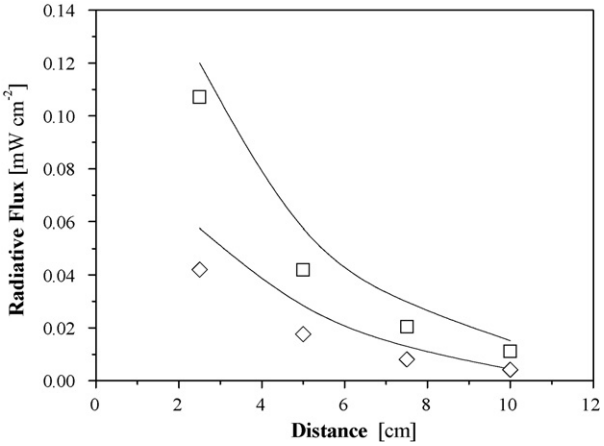

Fig. 6. Radiation flux obtained with two lamps (reflection effect). Experimental results obtained by using (□) a lamp turned off, (◊) a lamp envelope, and (–) predicted Monte Carlo values.

4.2.2. Two interposed lamps (shadowing effect)

This experiment (Fig. 1c) was described and analyzed in Section 3, and the experimental results were shown in Table 1. Fig. 5 shows the experimental results of the global transmittance for the quartz envelope, the UV-lamp turned off, and the UV-lamp turned on. The experimental results corresponding to the lamp off and on were used to estimate the absorption values of mercury at the vapor pressure inside the lamp. The parameters were adjusted in order to minimize the total square of the relative differences between model predictions and experimental results (objective function). The values obtained are as follows:

$$K_{\mathrm{Hg,lamp\ off}} = 0.46\,\mathrm{cm}^{-1} \quad (19)$$

$$K_{\mathrm{Hg,lamp\ on}} = 1.91\,\mathrm{cm}^{-1} \quad (20)$$

Utilizing these estimated values of K_{Hg}, the modeling results show good agreement with the experimental data. These parameters and the model were validated by predicting experimental data obtained under different conditions.

The global transmittance for the quartz envelope was also predicted using the model previously described. No adjustable parameters were required to predict this set of experimental values, because the mercury vapor is not involved in these experiments. The modeling results show good agreement with the experimental results.

4.2.3. Indirect radiation measurement (reflection effect)

Fig. 6 shows the experimental results obtained for the lamp configuration presented in Fig. 1d, described previously, and the model predictions under the same conditions. The model predictions obtained employing the estimated parameters (in this case, $K_{\mathrm{Hg,lamp\ off}}$) show good agreement with the experimental results. The global reflection of a lamp that is turned off is significantly higher compared to that of the quartz envelope. Again, these results show the importance of the mercury vapor in the optical behavior of the lamps.

4.2.4. Two adjacent lamps (additive effect)

Fig. 7 shows two sets of experimental results and the modeling predictions of the radiation flux against the distance of the detector and the center of the measurement chamber for two lamps at 5 cm apart from each other (Fig. 1e).

For one set of experiments, measurements were taken with the detector oriented towards the center of the chamber, with both lamps turned on. The predicted values agree with the experimental data, except near the center of the chamber, where large differences can be noted. These differences are due to the fact that the sensitivity of the radiometer decreases for beams reaching the detector with a high incident angle (the angle between the beam trajectory and the normal vector of the detector surface) [37]. When the sensor of the radiometer is located close to the center of the chamber, both lamps are beside it, and the radiation that reach the detector have a higher incident angle that this obtained when the detector is placed far from the lamps. Therefore, the poor agreement of the predicted and the experimental data when the detector is close to the center of the chamber may be a consequence of the limitation of the radiometer.

In order to overcome the aforementioned radiometer limitation, a second set of measurements was conducted with the detector oriented towards the center of one of the lamps (with the other lamp turned off). Then, the same procedure was carried out with the other lamp. In this way, the sum of the two experimental values obtained with the detector oriented towards each lamp would give the actual radiation flux, without the noted problem related to the reduction of radiometer sensitivity for radiation with high incidence angle. Fig. 7 shows the values obtained from

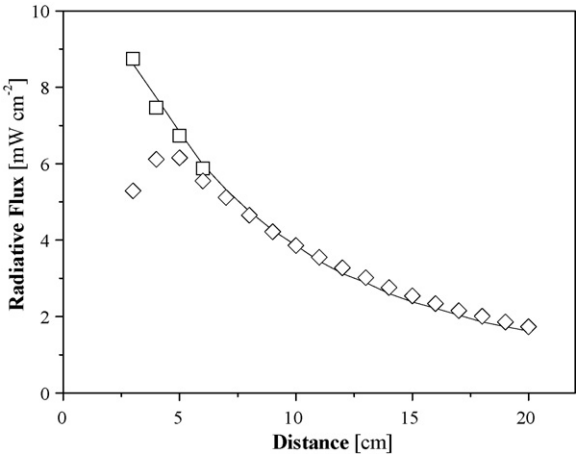

Fig. 7. Radiation flux obtained with two lamps (adding effect): (◊) experimental values obtained with the detector orientated to the center of the chamber, (□) sum of the experimental values obtained with the detector orientated to each lamp, and (–) predicted Monte Carlo values.

this second set of experiments at positions near to the center of the chamber, having good agreement with the model predictions of the two-lamp system. These results confirm that the cause of the error close to the lamp in the first set is related to the reduction of the radiometer sensitivity at relatively high incident radiation angle.

4.2.5. Three lamps

Fig. 8 shows modeling and experimental values of the radiation flux against the distance of the detector and the center of the measurement chamber for a three-lamp system (Fig. 1f). The predicted results show good agreement with the experimental data; however, when the detector is close to the lamps, the difference between the experimental and model increases. Again, the cause of the greater error near to the lamps can be attributed to the reduction of the radiometer sensitivity to the radiation that reaches the detector with high incident angles.

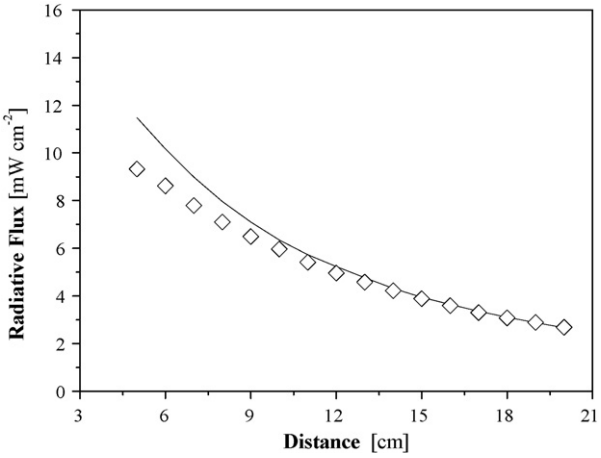

Fig. 8. Radiation flux obtained with three lamps: (◊) experimental values and (–) predicted Monte Carlo values.

4.3. Comparison between the complete and simplified models

The objective of this sub-unit is to compare the proposed radiation model with two simplified models, in which some assumptions have been applied in order to simplify the numerical solution for multi-lamp systems. For this, we consider (i) the complete radiation model, (ii) the ESVE model considering the lamps being 100% opaque (assumption employed by Jin et al. [14] and Yokota and Suzuki [30]), and (iii) the ESVE model considering the lamps being 100% transparent. Using any of these two assumptions, the complexity of the numerical solution is reduced significantly, since the angle-dependant reflectivity calculus, multiple-reflection, refraction, mercury vapor adsorption/re-emission are not involved. Two different scenarios were considered: three lamp system in air with opaque walls (Fig. 9a: model (i), c: model (ii), and e: model (iii)),

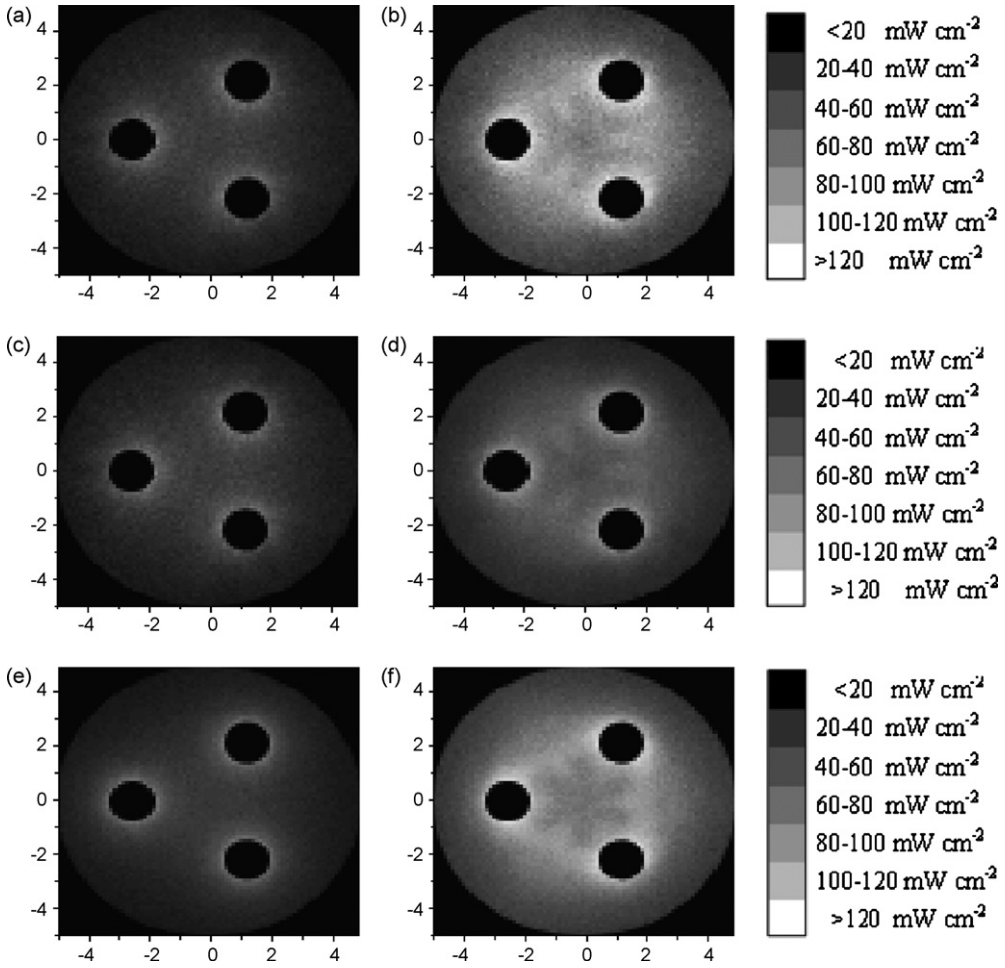

Fig. 9. Local incident radiation obtained by using three radiation models applied to two scenarios: opaque system walls (a, c and e) and reflective system walls (b, d and f).

and three-lamp reactor system in air with reflective walls (Fig. 9b: model (i), d: model (ii), and f: model (iii)). For the latter scenario, the reflectivity of the system walls was assumed to be equal to 50%. For the system with opaque wall, the average error among the three models is less than 2%, whereas in the system with reflective walls the predictions of the model that consider the lamps as opaque are 31% lower than the other model predictions. Note that the opaque lamps assumption (or 0% transmittance) is closer to the real transmittance of the lamps turned on (effective transmittance equal to 12%); however, this is a non-conservative assumption regarding the radiative energy. As was analyzed previously, the radiative energy that reaches a lamp is partially reflected, transmitted, or absorbed and re-emitted in a different direction. In this way, a transmittance value equal to 12% should not be interpreted as such that 88% of the radiative energy is absorbed in the lamp and disappears from the system, but that 88% of the radiation that reaches the lamp is reflected or absorbed/re-emitted, and leaves the lamp with a different direction from the original one. Taking this into consideration, neither the 100% opaque nor the 100% transmittance for the lamp would be a realistic assumption for a multi-lamp reactor. However, the 100% transmittance lamp assumption shows a better agreement with the complete model for the two particular scenarios analyzed. For the comparison, we chose the ESVE model because it is the most similar to the one we propose. However, considering that the results obtained from LSSE and ESVE models are very similar [32], the conclusions obtained considering the ESVE model would be valid to the LSSE model.

5. Conclusions

Experimental measurements of the radiation flux emitted by multi-UV lamps in different configurations have been obtained using a UV radiometer. The results indicated that the effective transmittance of the lamps was 12% when they are turned on, and 27% when they are turned off, whereas the effective transmittance of the lamp quartz envelope is 39%. These results show the importance of the effect of lamp shadowing, quartz reflection, and mercury vapor absorption and re-emission on the radiation field.

A multi-lamp model using the Monte Carlo method that takes into account the reflection/refraction on/in the lamps sleeves and the absorption/re-emission in the mercury vapor was able to predict the experimental results obtained under various conditions using one to three lamps in different configurations. For the lamp emission, the ESVE model was taken into account and the interaction between the lamps was considered using geometric optics. The single-reflection and multi-reflection in the quartz envelopes of the lamps were considered by using the Fresnel equation, and the refraction effect was considered by using the Snell law. The predicted values and experimental results showed good agreement.

Two simplified models that consider the lamp as 100% transparent and 100% opaque where compared with the proposed model under two different scenarios: a three-lamp reactor with opaque walls and a three lamp reactor with 50% reflective walls. The results indicate that 100% opaque lamp assumption could be considered for reactors whose walls are not reflective, whereas 100% transmittance lamp assumption could be employed for both reflective and non-reflective wall photoreactors. Nevertheless, in this work only two specific multi-lamp scenarios were analyzed and the conclusions cannot be extrapolated to every photoreactor. For a particular application, the most reliable assumption for the radiation model would be to take into account the reflection/refraction/absorption/re-emission effects in the lamps.

Acknowledgements

The authors are grateful to BI Pure Water (Canada) Inc., the Natural Sciences and Engineering Research Council of Canada (NSERC), Universidad Nacional del Litoral (UNL), and Consejo Nacional de Investigaciones Científicas y Técnicas (CONICET) for their financial support.

References

[1] L. Guzzella, S. Monarca, C. Zani, D. Feretti, I. Zerbini, A. Buschini, P. Poli, C. Rossi, S.D. Richardson, Mutat. Res. 564 (2004) 179–193.
[2] P. Andrzejewski, B. Kasprzyk-Hordern, J. Nawrocki, Desalination 176 (2005) 37–45.
[3] E.R. Blatchley III, K.C. Bastian, R.K. Duggirala, J.E. Alleman, M. Moore, P. Schuerch, Water Environ. Res. 68 (1996) 194–204.
[4] J.L. Braunstein, F.J. Loge, G. Tchobanoglous, J.L. Darby, Water Environ. Res. 68 (1996) 152–161.
[5] A.J. Oppenheimer, J.G. Jacangelo, J.M. Lane, J.E. Hoagland, Water Environ. Res. 69 (1997) 14–24.
[6] J.A. Guerrero-Beltrán, G.V. Barbosa-Cánovas, Food Sci. Technol. Int. 10 (2004) 137–147.
[7] W.A.M. Hijnen, E.F. Beerendonk, G.J. Medema, Water Res. 40 (2006) 3–22.
[8] D.A. Lyn, K. Chiu, E.R. Blatchley III, J. Environ. Eng. ASCE 125 (1999) 17–26.
[9] K. Chiu, D.A. Lyn, P. Savoye, E.R. Blatchley III, J. Environ. Eng. ASCE 125 (1999) 459–466.
[10] A. Sozzi, F. Taghipour, Ind. Eng. Chem. Res. 44 (2005) 9979–9988.
[11] S. Elyasi, F. Taghipour, Chem. Eng. Sci. 61 (2006) 4741–4749.
[12] B.F. Severin, M.T. Suidan, R.S. Engelbrecht, Water Res. 17 (1983) 1669–1678.
[13] M.D. Labas, R.J. Brandi, C.A. Martín, A.E. Cassano, Chem. Eng. J. 121 (2006) 135–145.
[14] S. Jin, K.G. Linden, J. Ducoste, D. Liu, Water Res. 39 (2005) 2711–2721.
[15] M.N. Ozisik, Radiative Transfer and Interactions with Conduction and Convection, Wiley, New York, 1973.
[16] M.G. Carvalho, T.L. Farias, Trans. IChemE: Part A 76 (1998) 175–184.
[17] V.K. Pareek, A.A. Adesina, AIChE J. 50 (2004) 1273–1288.
[18] M.M. Hossain, G.B. Raupp, Chem. Eng. Sci. 54 (1999) 3027–3034.
[19] M. Singh, I.S. Salvadó-Estivill, G. Li Puma, AIChE J. 53 (2007) 678–686.
[20] R. Changrani, G.B. Raupp, AIChE J. 46 (2000) 829–842.
[21] G.E. Imoberdorf, O.M. Alfano, A.E. Cassano, H.A. Irazoqui, AIChE J. 53 (2008) 2688–2703.
[22] G. Spadoni, E. Bandini, F. Santarelli, Chem. Eng. Sci. 33 (1978) 517–524.
[23] M. Pasqualli, F. Santarelli, J.F. Porter, P.L. Yue, AIChE J. 42 (1996) 532–537.
[24] Q. Yang, P.L. Ang, M.B. Ray, S.O. Pehkonen, Chem. Eng. Sci. 60 (2005) 5255–5268.
[25] A.E. Cassano, C.A. Martín, R.J. Brandi, O.M. Alfano, Ind. Eng. Chem. Res. 34 (1995) 2155–2201.
[26] S.M. Jacob, J.S. Dranoff, AIChE J. 16 (1970) 359–363.
[27] J.R. Bolton, Water Res. 34 (2000) 3315–3324.
[28] E.R. Blatchley III, Water Res. 31 (1997) 2205–2218.
[29] T. Akehata, T. Shirai, J. Chem. Eng. Jpn. 5 (1972) 385–391.
[30] T. Yokota, S. Suzuki, J. Chem. Eng. Jpn. 28 (1995) 300–305.
[31] H.A. Irazoqui, J. Cerda, A.E. Cassano, AIChE J. 19 (1973) 460–467.
[32] Y. Quan, S.O. Pehkonen, M.B. Ray, Ind. Eng. Chem. Res. 43 (2004) 948–955.
[33] V. Pareek, Int. J. Chem. Reactor Eng. 3 (2005) A56.
[34] R.B. Cundall, A. Gilbert, Photochemistry, Nelson, London, 1970.
[35] J.G. Calvert, J.N. Pitts Jr., Photochemistry, Wiley, New York, 1966.
[36] R. Siegel, J.R. Howell, Thermal Radiation Heat Transfer, 4th ed., Hemisphere Publishing Corp., Bristol, PA, 2002.
[37] B.F. Severin, P.F. Roessler, Water Res. 32 (1998) 1718–1724.